Available online at www.sciencedirect.com
SCIENCE DIRECT®
Journal of Nuclear Materials 326 (2004) 59–73
journal of nuclear materials
www.elsevier.com/locate/jnucmat

Fuel-to-cladding gap evolution and its impact on thermal performance of high burnup fast reactor type uranium–plutonium oxide fuel pins

Masaki Inoue *, Koji Maeda, Kozo Katsuyama, Kosuke Tanaka, Kenji Mondo, Masaki Hisada

Oarai Engineering Center, Japan Nuclear Cycle Development Institute, 4002 Narita-cho, Oarai-machi, Higashi-ibaraki-gun, Ibaraki-ken 311-1393, Japan

Received 28 January 2003; accepted 28 December 2003

Abstract

Drastic evolution of fuel-to-cladding gap is observed in high burnup JOYO Mk-II driver and MONJU type uranium–plutonium oxide fuel pins. The effect of the evolution is examined from viewpoints of fuel restructuring, gaseous FP release and retention and cesium migration behaviors. Its thermal impact on fuel pin performance is also studied by one-dimensional steady state thermal analysis. Threshold condition of the evolution depends on fuel pellet characteristics, burnup and probably temperature. The evolution directly relates to as-fabricated microstructures and to gaseous FP release and retention behavior. A comparison of fuel restructuring with predicted temperature profiles indicates that, even where large residual gaps are observed, non-gaseous filler always improves the heat transfer across the gaps.

PACS: 44.30.+v; 28.41.B

1. Introduction

Geometrical configurations of fuel pellet outer and cladding inner surfaces dominate both thermal and mechanical performances of fast reactor type uranium–plutonium oxide (FR-MOX) fuel pins. In a classical understanding for a typical fuel pin transverse section, at beginning-of-life a fuel pellet continuously swells to reduce a fuel-to-cladding gap width, at middle-of-life the gap becomes completely closed, and at end-of-life the larger swelling rate of a cladding than that of the fuel pellet results in a thermally detrimental gaseous gap. On the other hand, it is well known that large residual gaps filled with fission product (FP) compounds are observed even under unstrained cladding conditions in high burnup fuel pins. Tourasse et al. [1,2] named the large residual gaps as JOG (joint oxyde-gaine) for the Phenix fuel pins in 1992.

Tourasse et al. [1,2] comprehensively characterized the effect of fuel-to-cladding gap evolution and related phenomena including macro- and microscopic gaseous FP release and retention behavior, fuel restructuring and migrations of volatile elements and compounds. In this work, we call 'fuel-to-cladding gap evolution' as 'JOG evolution'. Maeda et al. [3] have also characterized microstructure and chemical features in context of the JOG evolution in high burnup FR-MOX fuels irradiated in the experimental fast reactor JOYO. However, the past studies [1–3] mainly focused on burnup dependence

* Corresponding author. Tel.: +81 29 267 4141x5713; fax: +81 29 267 1676/7130.
E-mail address: minoue@oec.jnc.go.jp (M. Inoue).

0022-3115/$ - see front matter © 2004 Elsevier B.V. All rights reserved.
doi:10.1016/j.jnucmat.2003.12.015

of the JOG evolution. So, the dependence on fuel pellet characteristics in the JOG evolution has not been experimentally revealed yet.

We have directed our attentions to thermal aspects on fuel pin performance much more than mechanical ones, because the JOG evolution will subsequently reduce the chances of fuel-to-cladding mechanical interaction. In spite of its importance, only Naganuma et al. [4,5] have performed thermal analysis for ultra high burnup fuel pins irradiated in the PFR, and pointed out that non-gaseous filler would preferably improve heat transfer across the gaps after the JOG evolution. Unfortunately, universality of the improvement has not been confirmed yet.

In this work, at first we examine JOYO Mk-II driver and MONJU type fuel pins to understand the influence of irradiation conditions and cladding strains on the JOG evolution. Secondly, the effect of fuel pellet characteristics on the JOG evolution is newly characterized. Thirdly, fuel restructuring, gaseous FP release and retention, and cesium migration behaviors involved in the JOG evolution are also characterized. Lastly, the impact of the JOG evolution on fuel pin thermal performance is quantitatively studied by one-dimensional steady state thermal analysis for transverse ceramographs.

2. Database

The Japan Nuclear Cycle Development Institute (JNC) has conducted a large number of irradiation tests in the JOYO and foreign fast reactors for JOYO Mk-II driver and MONJU type fuel pins [6]. We compiled the test results accumulated in the last two decades prior to this work [7].

A JOYO Mk-II driver fuel pin is clad with a modified SUS316 stainless steel (5.5 mm in outer diameter and 0.35 mm of wall thickness), filled with pure helium gas, and fueled with 550 mm in length. Nominal fuel pellet specifications of plutonium content (Pu/(U + Pu)), oxygen-to-metal (O/M) ratio, outer diameter and density are about 29 mass%, 1.97, 4.63 mm and 93–94% TD (theoretical density), respectively. Nominal diametral gap width is 170 μm. The fuel pellets are subdivided by raw powders into 'EP' (elemental plutonium dioxide powder) and 'MH' (co-converted power by microwave heating) types.

A MONJU type fuel pin for irradiation tests is clad with a modified SUS316 stainless steel (6.5 mm in outer diameter and 0.47 mm of wall thickness), and filled with pure helium gas with or without a tag gas capsule. Fuel column lengths are varied with core heights since the test fuel pins have been irradiated in several fast reactors (JOYO, Phenix, FFTF, etc.). Irradiation tests of the MONJU type fuel pin have been focused only on an outer core type fuel pin, so nominal fuel pellet specifications of Pu/(U + Pu), O/M ratio, outer diameter and density are about 30 mass%, 1.97, 5.40 mm and 85% TD, respectively. Nominal diametral gap width is 160 μm.

After the irradiations, test fuel pins were non-destructively inspected; particularly, cladding outer diameter profilometry and cesium-137 gamma scanning were performed to examine irradiation performance. The test fuel pins were punctured to analyze plenum gas compositions and macroscopic gaseous FP (krypton and xenon) release rates, and then sectioned to prepare transverse specimens. Fuel restructuring and residual diametral gap width were measured in photo mosaics of ceramographs in as-polished and/or after-etched conditions. We define a residual gap width as a distance between fuel pellet outer and cladding inner surfaces, and average eight measurements in different circumferential locations in each transverse section. Chemical compositions of gap filler and radial concentration profiles of retained xenon in fuel pellets were analyzed by electron probe micro analysis (EPMA).

It is very fortunate that non-destructive and destructive examination results for thirty JOYO Mk-II driver fuel pins, listed in Table 1, are available to characterize the dependence on fuel pellet characteristics in the JOG evolution. These eligible fuel pins load four EP type (C5J-005, C5J-006, C5J-007, FM2-312) and three MH type (C5J-001, C5J-002, C5J-003) fuel pellet lots which are varied with grain diameter and stoichiometry, and were irradiated without in-core shuffling up to 60–70 GWd/MTM in fuel pin average in the JOYO. Fuel pellets loaded in each fuel pin is from the same lot. Especially, C5J-006 (O/M ratio: 1.99) and C5J-007 (O/M ratio: 1.95) is originally from the same lot, but C5J-007 is additionally reduced to lower O/M ratio at 1773 K for 18 h in nitrogen–hydrogen atmosphere [8]; these two fuel pellet lots have identical as-fabricated microstructures but different O/M ratios.

3. Dependence on irradiation conditions and cladding strains

Residual diametral gap widths are plotted versus local burnups and cladding inner diameter changes (cladding strains) in Fig. 1 for the JOYO Mk-II driver and in Fig. 2 for the MONJU type fuel pins, and their axial distributions are shown in Fig. 3.

The residual gap widths decrease with burnup up to 50 GWd/MTM consistently with the classical understanding. However, some ceramographs show large residual gap widths, which are greater than a half of as-fabricated ones, beyond 50 GWd/MTM in both JOYO Mk-II driver and MONJU type fuel pins. For transverse ceramographs with large residual gaps, we suspect the JOG evolution by the following two criteria; (a) its local burnup is higher than 50 GWd/MTM; (b) the

Table 1
As-fabricated fuel pellet specifications and irradiation conditions of the JOYO Mk-II driver fuel pins for the detailed investigations

Fuel pellet lot ID	Type of raw powder	Lot mean			Grain diameter (μm)		Fuel pin no.	Transverse ceramograph[a] (shown in Figs. 5 and 8)	Linear heat rate (pin average) at end-of-irradiation (kW/m)	Burnup (pin average) at end-of-irradiation (MWd/MTM)
		Pu content Pu/(Pu + U) (mass%)	Uranium-235 enrichment (mass%)	O/M ratio						
C5J-001	MH	28.80	18.5	1.97	13	1	G051	–	22.3	60 105
						2	G058	J1	23.4	62 815
						3	G034	–	24.2	65 316
						4	G031	–	24.7	67 356
						5	G041	–	24.8	67 634
C5J-002	MH	28.57	18.2	1.96	8	6	G060	–	22.4	60 893
						7	G067	–	23.1	62 763
						8	G045	–	23.7	64 565
C5J-003	MH	28.74	18.3	1.94	14	9	G039	–	22.5	61 213
						10	G068	–	22.7	61 954
						11	G035	–	23.5	64 295
						12	G053	J2	24.1	66 246
C5J-005	EP	27.33	18.0	1.97	24	13	G069	–	22.4	60 072
						14	G048	–	22.8	61 203
						15	G074	–	23.2	62 698
						16	G056	–	23.4	62 978
						17	G010	–	23.4	63 031
						18	G024	J3	23.8	64 303
C5J-06[b]	EP	27.54	18.5	1.99	10	19	G050	–	22.6	60 615
						20	G076	–	23.1	62 133
						21	G046	–	23.7	63 775
						22	G043	J4	24.3	65 938
C5J-007[b]	EP	27.54	18.5	1.95	10	23	G047	–	23.7	63 487
						24	G017	–	24.1	64 875
						25	G064	J5	24.3	65 519
FM2-312	EP	29	18.6	1.99	–	26	E354	–	31.4	67 750
						27	E353	–	31.7	68 080
						28	E352	–	31.9	68 530
						29	E359	J6–J10	32.0	68 760
						30	E351	–	32.1	69 110

[a] Not all fuel pins were provided for ceramographic works.
[b] Siblings.

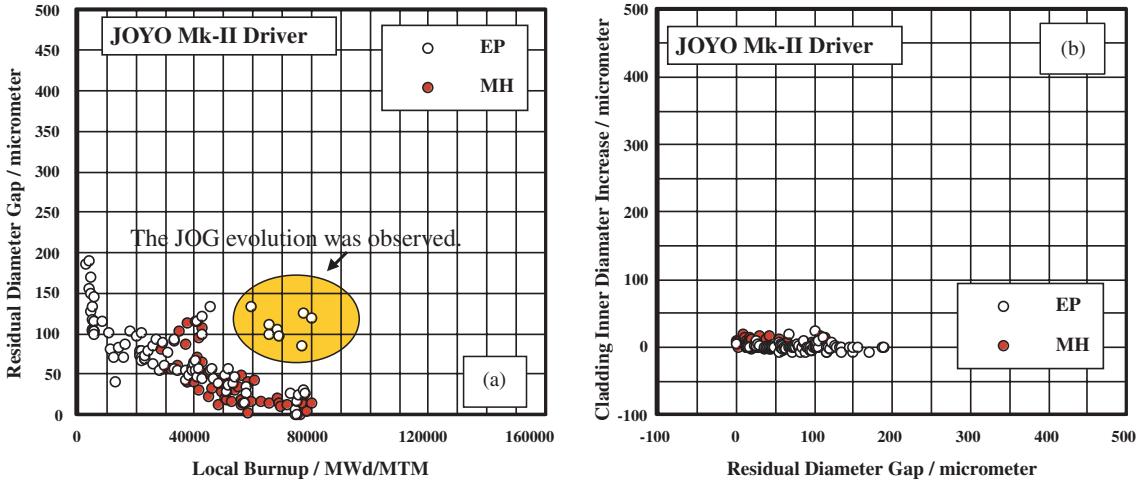

Fig. 1. Burnup and cladding strain dependence of fuel-to-cladding residual gaps in the JOYO Mk-II driver fuel pins.

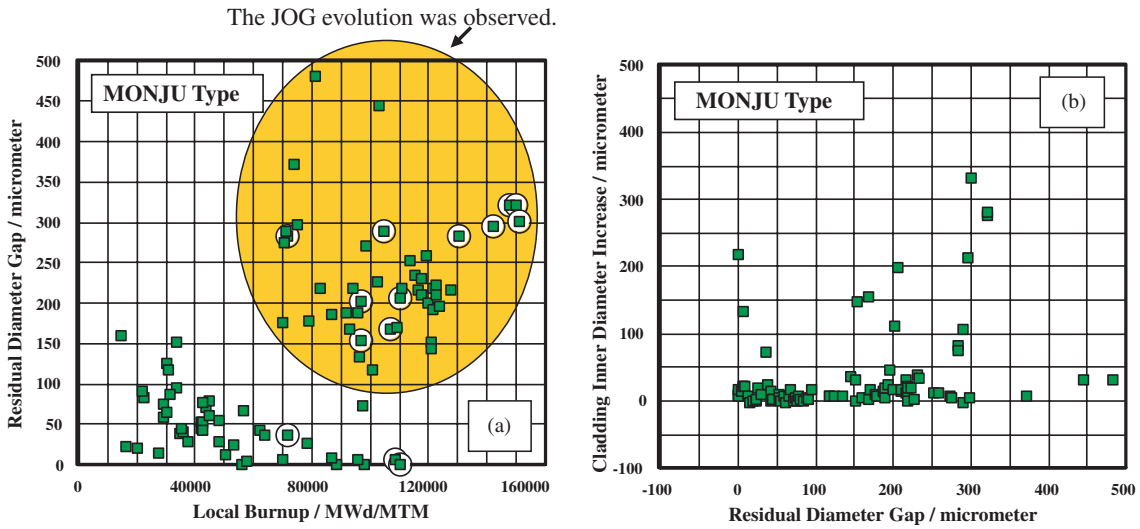

Fig. 2. Burnup and cladding strain dependence of fuel-to-cladding residual gaps in the MONJU type fuel pins.

residual gap width is larger than a half of as-fabricated nominal diameter gap width. The suspected specimens are circled in Figs. 1(a), 2(a) and 3(a), (c) and (d). The residual gap widths after the JOG evolution of the MONJU type are larger than those of the JOYO Mk-II driver fuel pins.

All of the JOYO Mk-II driver fuel pins ended their irradiations without cladding swelling as shown in Fig. 1(b). Therefore, the JOG evolution occurs under unstrained cladding conditions similarly to the high burnup Phenix fuel pins. In the MONJU type fuel pins, cladding diameter changes are almost equal to residual diametral gap widths in some ceramographs but much less in the others as compared in Fig. 2. At present, the effect of cladding lift-off and restraint on the JOG evolution is not clear. As can be seen in Figs. 1 and 2, threshold burnup of the JOG evolution is higher than 50 GWd/MTM similarly to the high burnup Phenix fuel pins. The threshold burnup for the JOYO Mk-II driver fuel pins appears to be lower than that of the MONJU type fuel pins.

We examine the JOG evolution for local burnups and cladding inner temperatures in Fig. 4. Needless to say, temperatures around fuel pellet peripheral regions especially before the JOG evolution reflect cladding ones. Threshold cladding inner temperature appears to

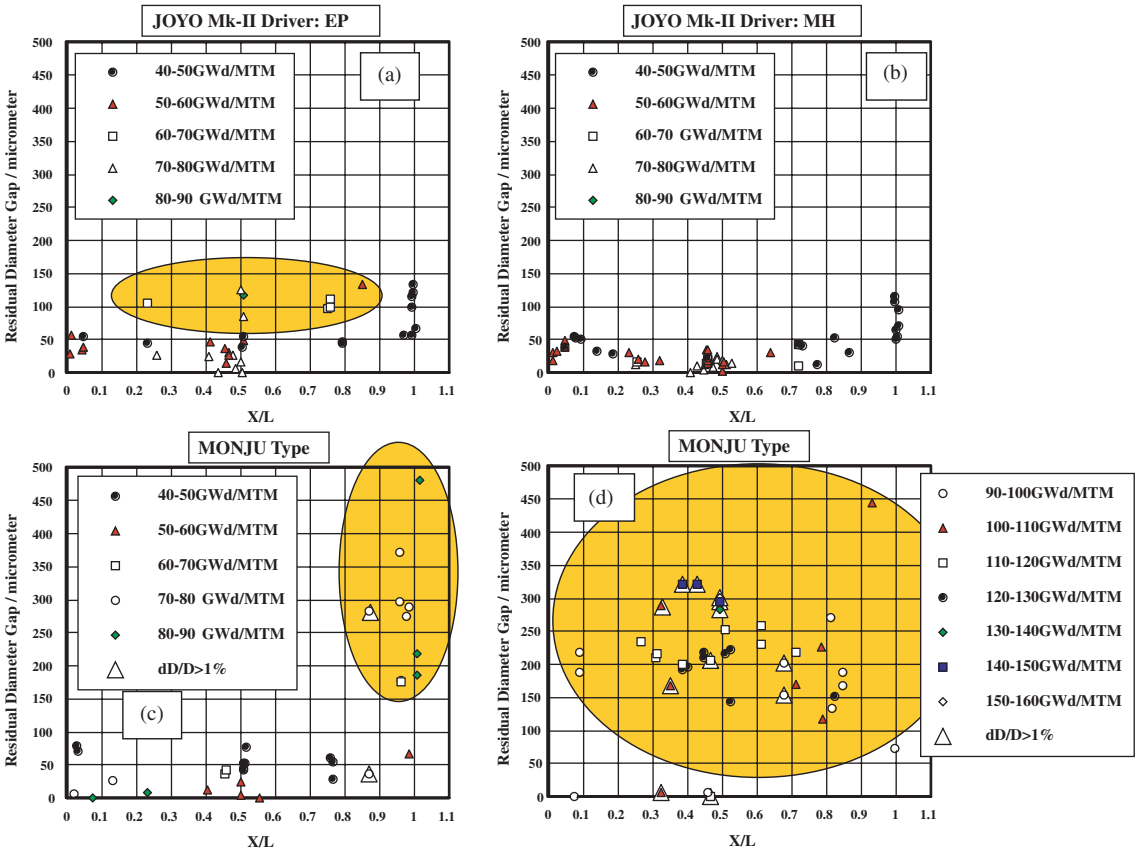

Fig. 3. Axial distribution and burnup dependence of the JOG evolution in the JOYO Mk-II driver and MONJU type fuel pins.

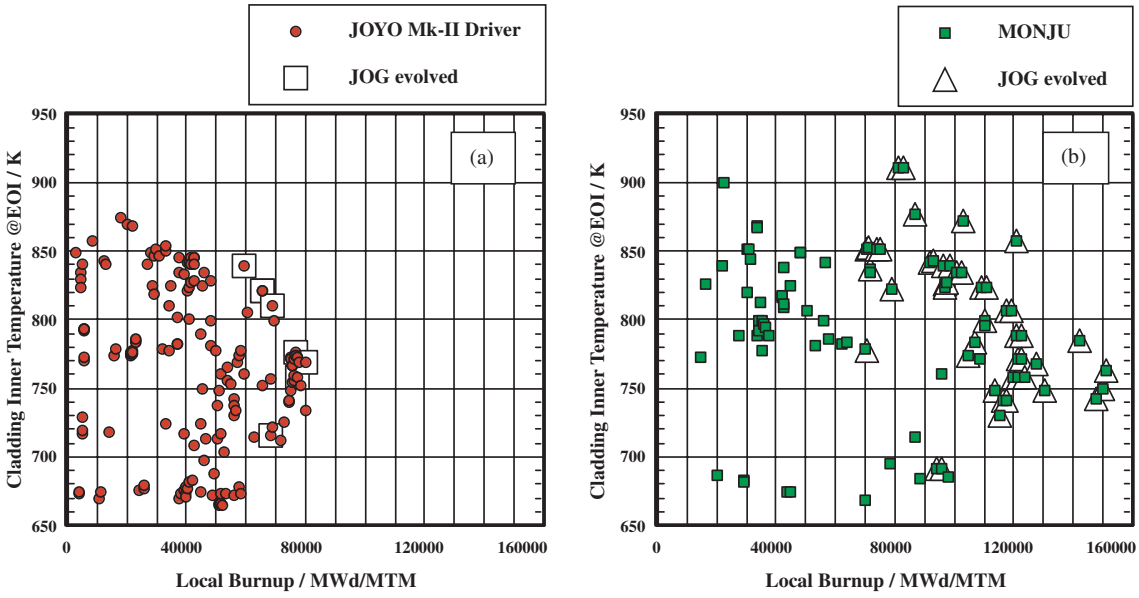

Fig. 4. Mapping of the JOG evolution versus burnups and cladding temperatures.

exist since the JOG evolution tends to occur in upper part of fuel column. Even if local irradiation conditions are almost equal to each other, some show the JOG evolution and the others do not. Particularly in the JOYO Mk-II driver fuel pins, the JOG evolution is observed only in the EP type. These features indicate that fuel pellet characteristics also affect the JOG evolution. So, dependence on the fuel pellet characteristics will be characterized in the next chapter.

4. Dependence on fuel pellet characteristics

Five transverse ceramographs: J1 through J5, which are loaded with different fuel pellet lots designated as 'C5J-' (see Table 1), are shown in Fig. 5. These specimens were irradiated at almost equal conditions in both burnups (75–77 GWd/MTM) and cladding temperatures as listed in Table 2. J4 and J5 show the JOG evolution but J1, J2 and J3 do not. As already mentioned in Chapter 3, the JOG evolution is observed only in the EP types (J4 and J5) not in the MH types (see J1 and J2). It is definitely evident that fuel pellet characteristics also affect the JOG evolution.

Katsuyama et al. [9] have characterized the effect of the raw powders on irradiation behaviors, and revealed that porosity distributions in the EP and MH types are different each other, that the fuel pellet matrix of the MH type is denser due to the higher sinterability than that of the EP type, and that the EP types exhibit larger fission gas release rates than the MH types. Macroscopic gaseous FP release rates loaded with seven different fuel pellet lots of the JOYO Mk-II driver fuel pins listed in Table 1 are compared in Fig. 6. As can be seen in Figs. 5 and 6, the difference of the raw powder influences both gaseous FP release and JOG evolution behaviors.

Although J3 is loaded with the EP type, it does not show the JOG evolution. This means that another parameter influences the JOG evolution. In three specimens with the EP types, the smaller grain diameter fuel pins (C5J-006: J4 and C5J-007: J5) show the large residual gaps, but the largest one (C5J-005: J3) does not. From another viewpoint, the larger grain diameter in the EP types exhibits the lower release rate as shown in Fig.

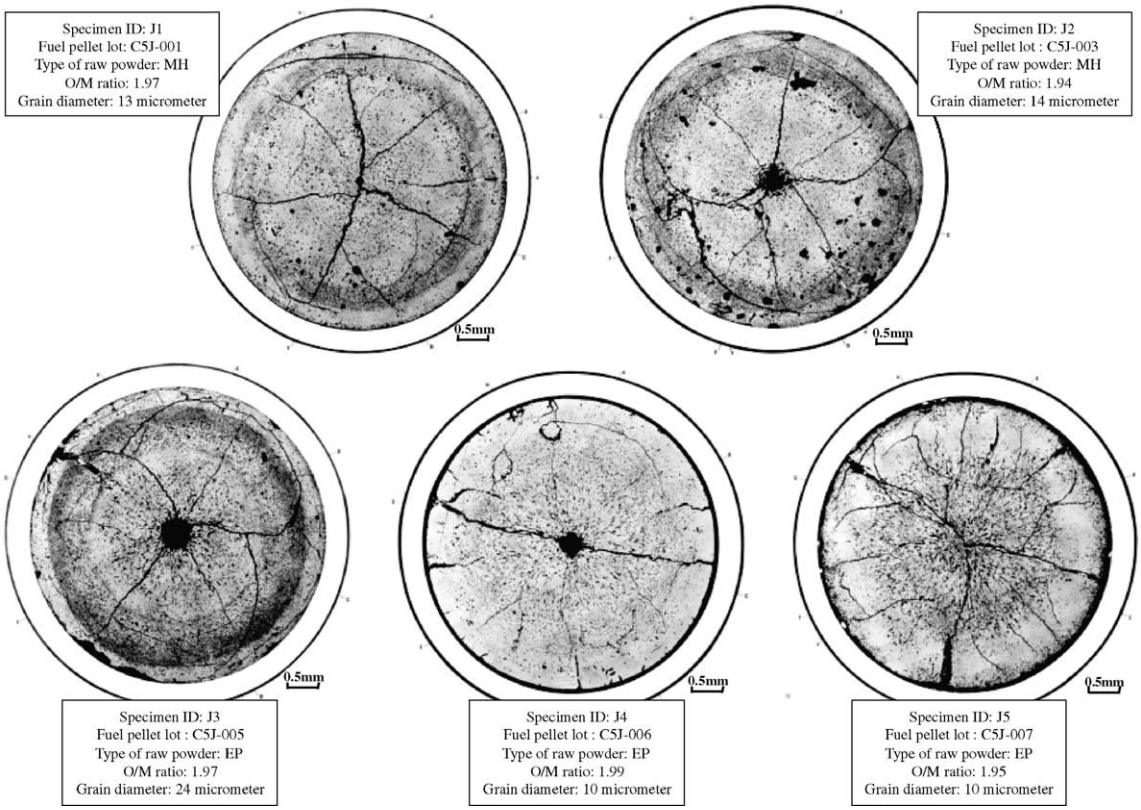

Fig. 5. Transverse ceramographs at core mid-planes in the JOYO Mk-II driver fuel pins loaded with different fuel pellet lots.

Table 2
Local irradiation conditions of transverse specimens for ceramographs and electron micro-probe analysis

Specimen ID	Fuel pellet lot ID	Fuel pellet type	DFCB[a] (mm)	Linear heat rate at beginning-of-irradiation (kW/m)	Cladding midwall temperature at beginning-of-irradiation (K)	Linear heat rate at end-of-irradiation (kW/m)	Cladding midwall temperature at end-of-irradiation (K)	Burnup (MWd/MTM)	JOG evolution
J1	C5J-001	JOYO Mk-II Driver	275	34.4	783	27.9	759	76 400	No
J2	C5J-003	JOYO Mk-II Driver	260	34.1	777	27.6	754	76 461	No
J3	C5J-005	JOYO Mk-II Driver	273	33.8	784	27.5	760	75 119	No
J4	C5J-006	JOYO Mk-II Driver	275	34.7	785	28.1	760	77 069	Yes
J5	C5J-007	JOYO Mk-II Driver	278	34.5	786	27.9	761	76 454	Yes
J6	FM2-312	JOYO Mk-II Driver	23	26.5	665	23.0	665	57 669	No
J7	FM2-312	JOYO Mk-II Driver	142	34.2	718	28.4	709	72 944	No
J8	FM2-312	JOYO Mk-II Driver	276	37.7	772	30.8	752	80 045	Yes
J9	FM2-312	JOYO Mk-II Driver	412	31.8	825	26.8	796	68 806	Yes
J10	FM2-312	JOYO Mk-II Driver	547	20.1	848	18.2	816	45 236	Yes

Out-to-in shuffling experienced.
[a] Distance from core bottom.

6 similarly to water reactor fuels reported by Une et al. [10]. It is evident that grain diameter influences the JOG evolution. In C5J-006 and C5J-007, it appears that the burnup dependence of the release rates are equivalent, that the JOG evolution are observed in highest burnup fuel pins, and that the effect of the stoichiometry is not distinguishable. The dependencies on the raw powders and grain diameters mentioned above indicate that the JOG evolution directly relates to as-fabricated microstructures and to the gaseous FP release and retention behavior.

5. Dynamic changes involved in the JOG evolution

Axial gamma scan profiles of cesium-137 intensities of five JOYO Mk-II driver fuel pins (E351–E354 and E359) loaded with 'FM2-312' fuel pellet lot (EP type) are compared in Fig. 7(a)–(e). Pin powers and resultant burnups are different slightly with the distance from the core center as noted in Table 1 and Fig. 7. The lowest burnup fuel pin (E354) exhibits an almost identical profile to its power one and little cesium axial migration. In contrast, the higher burnup fuel pins exhibit the larger extent of the perturbation which means more significant axial migration of cesium. Also, the more gaseous FP is released to plenum in the higher burnup fuel pin as shown in Fig. 6.

Five transverse ceramographs (J6–J10) at different axial locations in the E359 pin are shown in Fig. 8, and their irradiation conditions are tabulated in Table 2. In J6 and J7 the gaps are completely closed, but J8, J9 and J10 show the JOG evolution. Burnups of J7 and J9 are almost equal to each other (70 GWd/MTM), but cladding mid-wall temperature of J9 (796 K) is higher than J7 (709 K) because J7 and J9 locates almost opposite sides of the core mid-plane (distances from core mid-plane are about 135 mm as listed in Table 2). The difference between J7 and J9 means that the threshold condition of the JOG evolution depends on temperature. As compared in Fig. 7(d), the JOG evolution is observed only in a perturbed extent in its profile. The explanation is that the JOG evolution also involves the axial migration of cesium. We confirm that the JOG evolution involves the dynamic changes of the gaseous and volatile FP release and retention similarly to the high burnup Phenix fuel pins.

We think that the profile changes in Fig. 7 animate the JOG evolution with burning. Since a burning rate of the fuel pins is about 190 MWd/MTM a day, we can expect that the JOG evolution probably occurs in shorter than a week. Furthermore, since the perturbations appear to start in upper half of fuel columns, this also implies that the threshold condition of the JOG evolution depends on temperature.

Radial xenon retention profiles in five transverse sections shown in Fig. 8 are plotted in Fig. 9. It should be mentioned here that xenon production rate is homogeneous over every transverse section since there is no radial power depression in test fuel pins irradiated in the JOYO. It is noticeable that the retained xenon concentrations in peripheral regions decrease drastically with the JOG evolution; much less xenon in peripheral region is retained in J9 than in J7. A dip around dark ring region appears in J7 probably results from fuel pellet cracks or specimen chipping.

Maeda et al. [3] reported that highly porous and very fine crystalline microstructures are evolved in fuel pellet

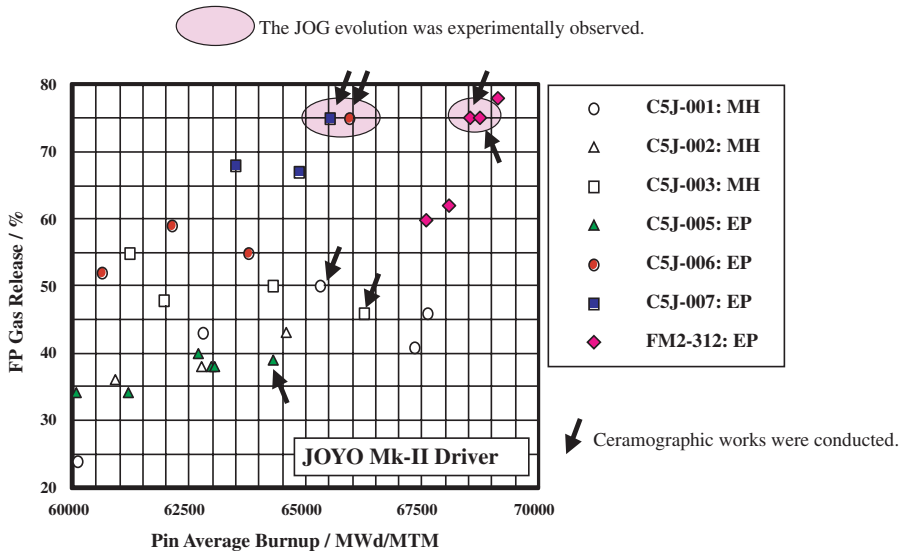

Fig. 6. Gaseous fission product release rates to the plenum in comparison with fuel pellet lots and burnups.

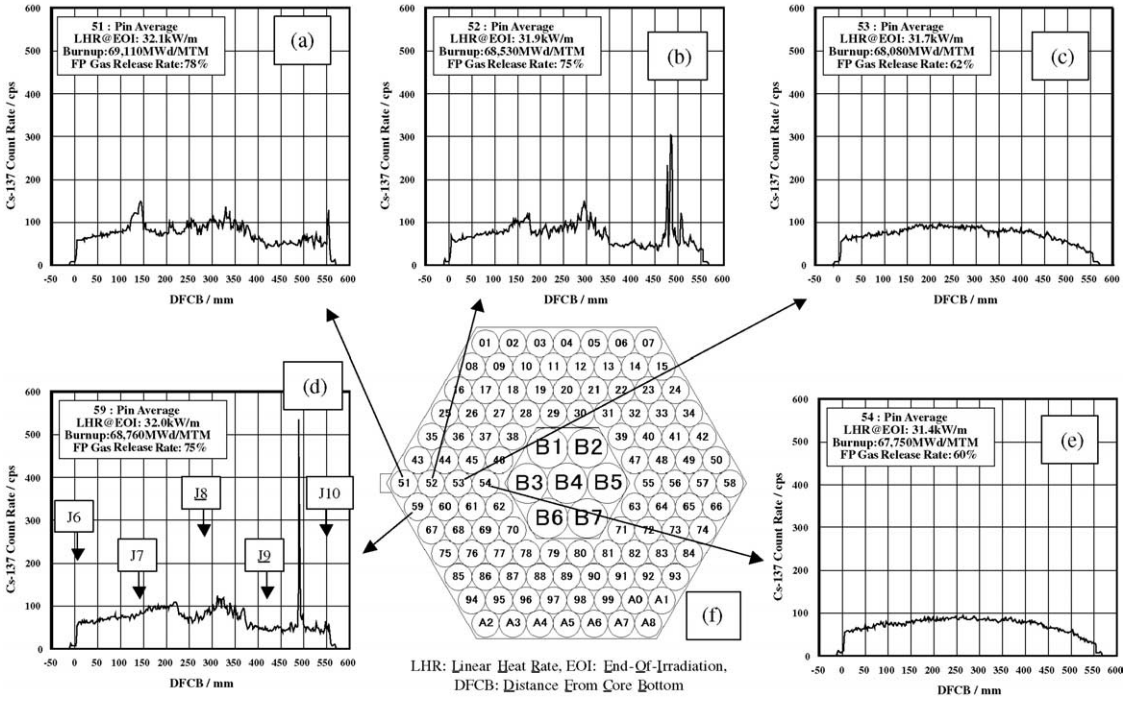

Fig. 7. Cesium axial distribution changes during slight burnup increases in the JOYO Mk-II driver fuel pins.

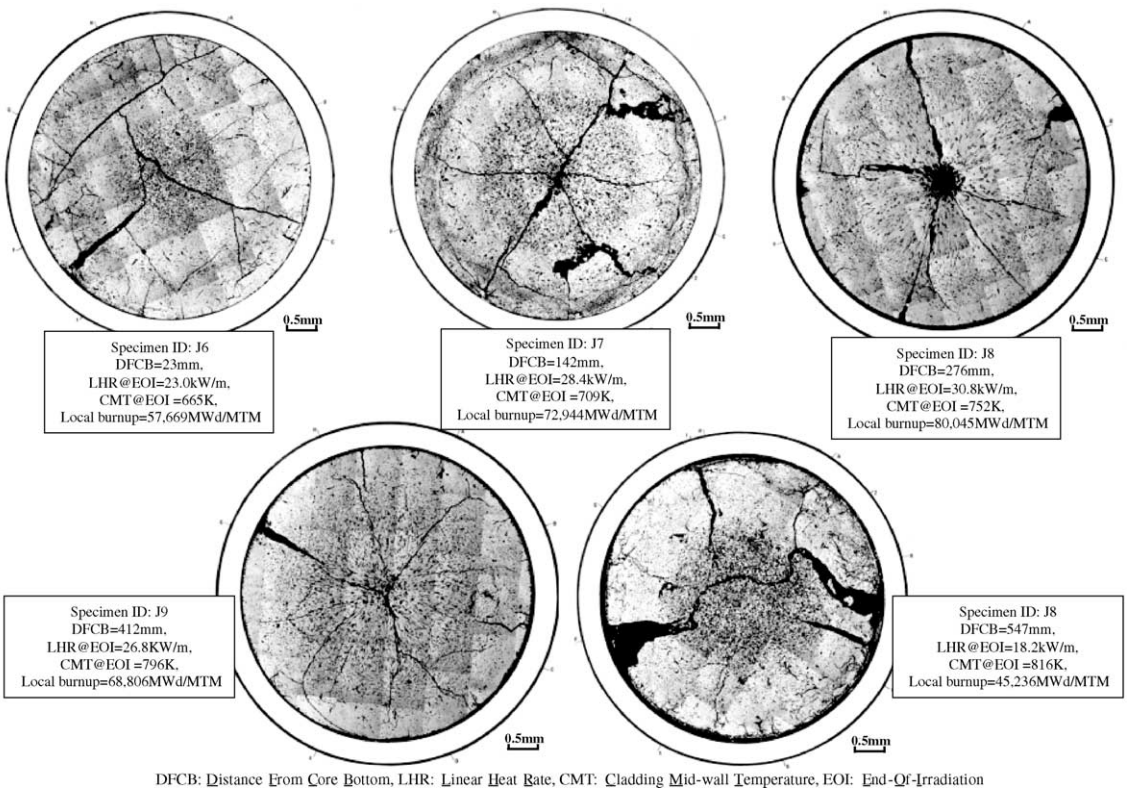

Fig. 8. Transverse ceramographs at different axial locations in JOYO Mk-II driver fuel pin.

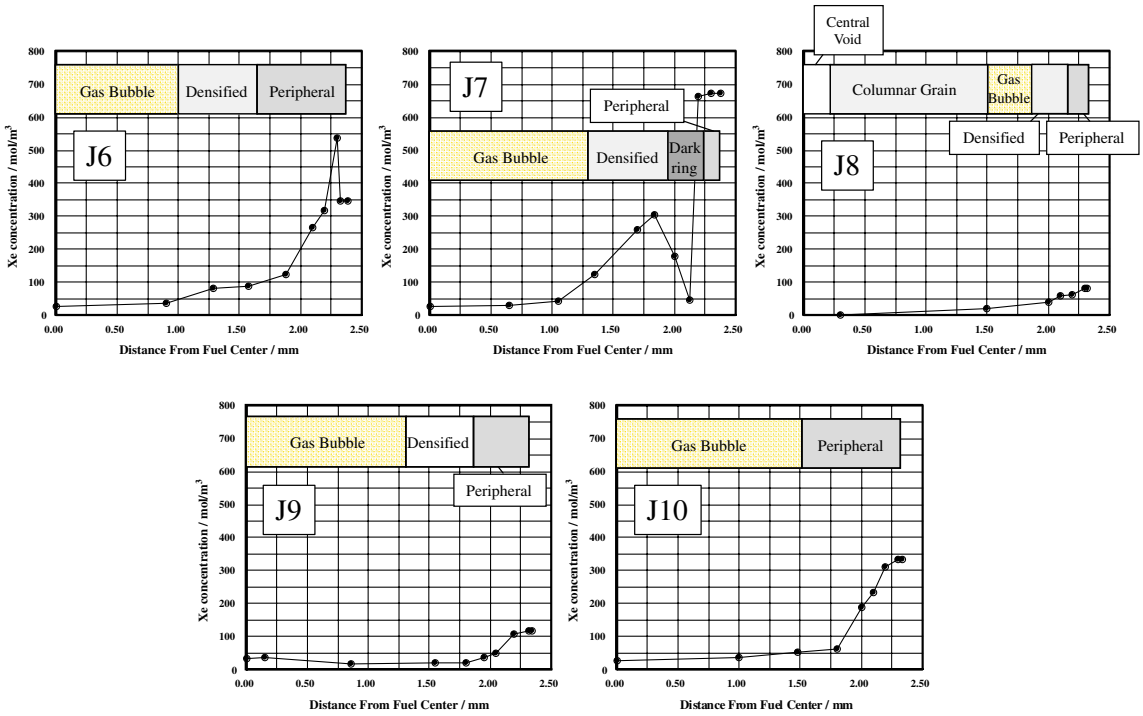

Fig. 9. Radial xenon retention profiles at different axial locations in the JOYO Mk-II driver fuel pin.

peripheral regions where fuel pellet and cladding are in contact, but fuel peripheral region becomes much less porous after the JOG evolution When compared J4, J5, J8 and J9 with J1, J2 and J3 in Figs. 5 and 8, the JOG evolution also involve additional fuel restructuring which have the following dynamic changes; precipitated metallic inclusions are more distinguishable; the pores in the inner regions are arranged toward the fuel pellet center.

We suspect that the dynamic changes of the release and retention behaviors as well as the fuel restructuring in peripheral regions are probably induced by transient temperature increase. The suspected causes of the transient temperature increase will include the gas blanketing of the gap. However, we should emphasize that, even though the transient temperature increase occurs under steady state irradiations (constant power), it will not be sufficiently high and long to cause lenticular void formations and its migrations.

In addition to the JOG evolution, we should pay much more attentions to dynamic changes of gaseous FP release and retention behaviors. Maeda et al. [3] found out that gaseous FP retentions in fuel matrix abruptly decreased around 70 GWd/MTM. Tourasse et al. [1] also reported that the amount of the retained gaseous FP in the fuel pellet showed a remarkable 'dip' between 70 and 90 GWd/MTM corresponding to the JOG evolution. These observations are coincident with those on high burnup uranium dioxide fuels in thermal reactors reported by Walker et al. [11] and Lassmann et al. [12]. We will continue to investigate the JOG evolution scenario in conjunction with the dynamic changes of the gaseous FP release and retention behavior in future.

6. Thermal impact of the JOG evolution on fuel pin performances

6.1. Procedure of thermal analysis

As described in the previous chapter, the JOG evolution probably accompanies the transient temperature increase. At present, it is impossible to calculate fuel temperature history during the JOG evolution, because we have not understood its scenario and kinetics in detail yet. However, we can confidently evaluate transverse ceramographs after the JOG evolution for radial temperature profiles by thermal analysis especially at end-of-irradiation (EOI) conditions. Fuel restructuring is always the effect of irradiation and temperature histories and grain growth and lenticular void (columnar grain) formation have known threshold temperatures. So, we can confirm the liability of the calculations.

We make one-dimensional steady state thermal analysis by a FORTRAN program in a similar manner

performed by Naganuma et al. [4,5]. Detailed description of the program can be found in Appendix A and furthermore in the reference [7]. Thermal expansions of fuel pellet and cladding and resultant gap shrinkages are appropriately considered to calculate temperature increments both across the gap and over the fuel pellet by an iterative method in the program. In the analysis, fuel surface and fuel center temperatures only at EOI conditions are calculated for all transverse ceramographs where the JOG evolution and fuel restructuring are measured. The JOG evolution also changes heat transfer medium across the gap. So, ingredients of gap filler are selected as a parameter for the analysis. We assume two species of gap filler which are cesium molybdate (JOG case) or mixed gas (gas case). Chemical compositions of the mixed gas are experimentally determined by fuel pin puncture tests. Johnson et al. [13] have predicted that cesium molybdate (Cs_2MoO_4) would be thermodynamically stable in the gaps in high burnup FR-MOX fuel pins. The main components of the JOG were determined to be cesium and molybdenum by Tourasse et al. [1,2], Maeda et al. [3] and Naganuma et al. [4,5]. The calculations by the JOG case will provide temperature profiles when the JOG evolution is

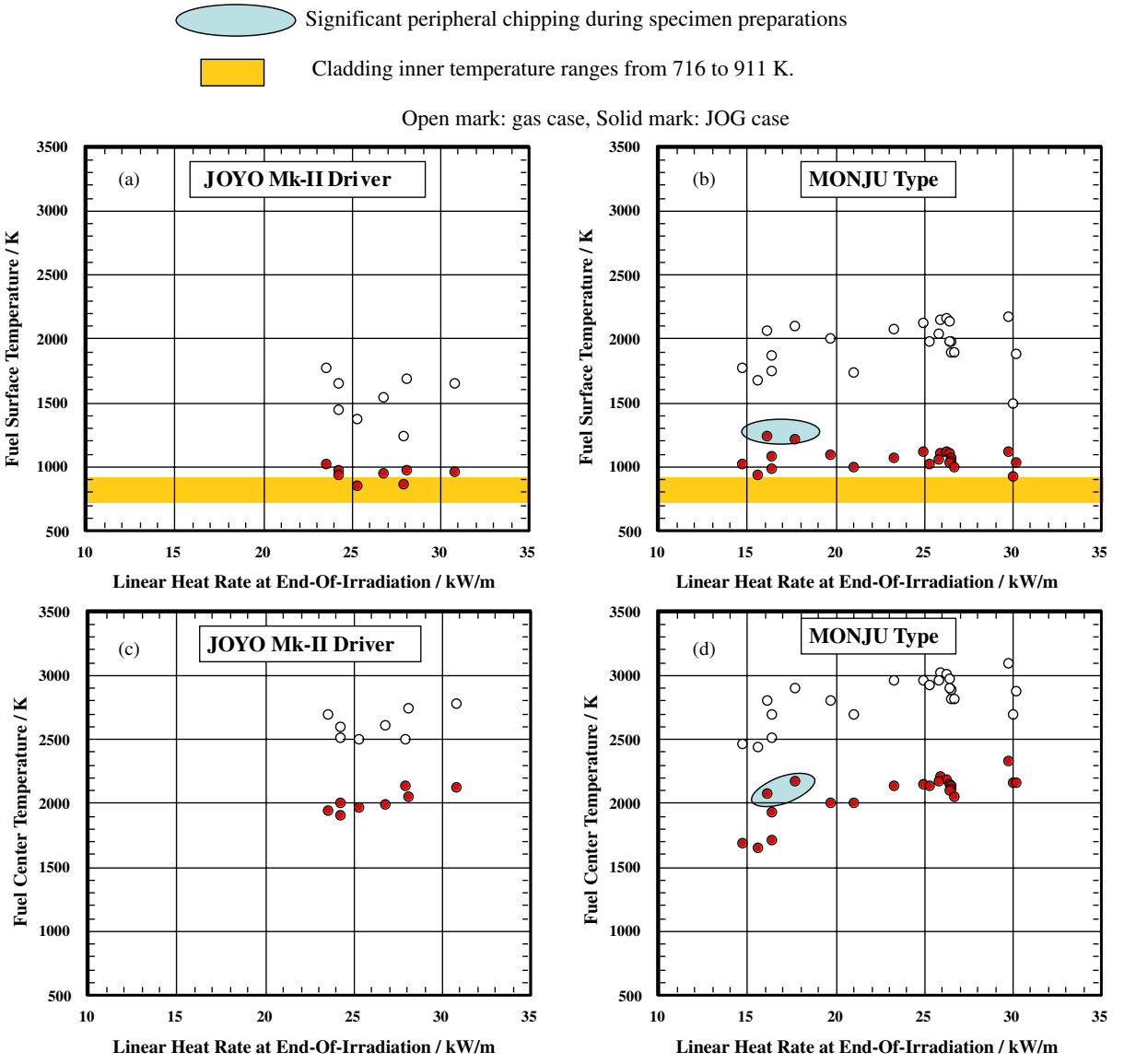

Fig. 10. Fuel surface and center temperatures calculated for the transverse ceramographs with the JOG evolution in the JOYO Mk-II driver and MONJU type fuel pins.

matured. On the other hand, the calculations by the gas case will provide temperature profiles when the gap is filled only with the mixed gas, in other words, fully gas-blanketed. We expect that the JOG case will be the lower bounds and the gas case be the upper bounds during the JOG evolution.

6.2. Consistency with fuel restructuring

Calculated fuel surface and fuel center temperatures are plotted versus local linear heat rates at EOI conditions in Fig. 10. In the gas case (open marks), fuel center temperatures are always higher than 2400 K. By contrast, in the JOG case (solid marks), fuel center temperatures range from 1600 to 2200 K. Fuel center temperatures by the JOG case depend more clearly on local linear heat rates and show smaller scatters than those by the gas case. It is remarkable that temperature increments across the gap in the gas case (472–1414 K) are four to six times as high as those in the JOG case (93–372 K).

In the JOG case, calculated fuel center temperatures are lower than the threshold temperature of the columnar grain formation believed to be over 2100 K. Since fresh (as-evolved) columnar grains are never observed in the ceramographs with the JOG evolution, we conclude that the JOG case is reasonably consistent with fuel restructuring for EOI conditions. Therefore, even where large residual gaps are observed, non-gaseous filler *always* improves the heat transfer across the gaps.

Fuel surface and fuel center temperatures by the gas case are enough high to cause the additional fuel restructuring mentioned in Chapter 5, radial and axial migrations of volatile FPs, and disappearance of fission gas bubbles in peripheral regions. The transient temperature increase induced by the gas blanketing is probable to explain the dynamic changes involved in the JOG evolution.

6.3. Indication of thermodynamic thresholds

It is obvious that fuel surface temperature in the JOG case show little local linear heat rate dependence. Actually, the average of fuel surface temperatures of the JOG case is 943 K (one standard deviation is 55 K for eight points) in the JOYO Mk-II driver and 1050 K (one standard deviation is 59 K for 20 points) in the MONJU type fuel pins. Even though fuel pin geometries are different, both averages appear to be close to the boiling point (976 K) of metallic cesium. This suggests that evaporation and condensation behavior of cesium in element and compounds relates to the JOG evolution. Also, fuel pellet surfaces after the JOG evolution appear to be always symmetrical. In fuel-to-sodium reactions in failed fuel pins, radial oxygen potential profile controls the reaction product formation, and the reacted layer thickness depends largely on the heat flux which is a function of fission density and fuel pin geometry. The larger residual gap width after the JOG evolution in the MONJU type than the JOYO driver fuel pins indicates the influence of heat flux. It is likely that fuel-to-sodium reaction behavior is similar to the JOG evolution. The residual gap widths with the JOG evolution would depend on the heat flux and have threshold conditions determined by chemical thermodynamics. The thermodynamic analysis will provide further understandings of mechanism and threshold conditions for the JOG evolution.

7. Conclusions

In this work, the dependence of the JOG evolution on irradiation conditions and cladding strains together with the fuel pellet characteristics in the JOYO Mk-II driver and MONJU type fuel pins are extensively examined. In addition, fuel restructuring, macroscopic and microscopic gaseous FP release and retention and cesium migration behaviors involved in the JOG evolution are characterized.

The JOG evolution and related phenomena observed in this work agree well with the past studies [1–3]. Additionally, we newly find out the following three features: (i) the threshold condition of the JOG evolution depends not only on burnup but also probably on temperature; (ii) the JOG evolution is expected to be a very short term phenomenon; actually it will take shorter than a week; (iii) the JOG evolution directly relates to grain morphology which is very similar to the relation between the gaseous FP release and retention behavior. It is noteworthy that these three features combine microstructure evolution with transition of gaseous FP release and retention in high burnup oxide fuels. Further investigations of the JOG evolution will contribute to understand high burnup behaviors of both FR-MOX and thermal reactor type oxide fuels.

Microstructure features on the peripheral regions indicate that the transient temperature increase is probably induced by the JOG evolution even under the steady state irradiations but not sufficient to cause the lenticular void formation and its migration. The one-dimensional steady state thermal analysis for the transverse ceramographs with the JOG evolution is conducted to evaluate the impact of the JOG evolution on fuel pin thermal performances. The comparison of the fuel pellet restructuring with temperature profiles indicates that, even where large residual gaps are observed, in other words, after the JOG evolution, non-gaseous filler always improves the heat transfer across fuel-to-cladding gaps.

We will continue to investigate the JOG evolution in conjunction with the dynamic changes of the gaseous FP

release and retention behavior in order to establish/identify the JOG evolution scenario/mechanism in future.

Acknowledgements

The advice of Mr Takeo Asaga and Dr Shigeharu Ukai is acknowledged. Also the assistance by Mr Junichi Nemoto, Mr Masahiro Ito and Mr Ikuo Ishitani in the thermal analysis is acknowledged. Ceramograph and electron micro-probe analysis works in the Fuel Monitoring Facility were conducted in the grateful cooperation with Mr Yukihiro Ohsato, Mr Sadayoshi Nukaga and Mr Yasuhiro Onuma.

Appendix A. Thermal modeling of radial heat flow in irradiated fuel pins

A.1. Calculation tool for this analysis

A FORTRAN program is used for one-dimensional steady state thermal analysis. Prior to the analysis radial heat flow in high burnup fuel pins is modeled and incorporated into the program as described in Sections A.3, A.4, and A.5. Contrary to fuel pin performance analysis codes, the program cannot calculate temperature histories. However, the program can sufficiently consider radial heat flows inside fuel pins; in particular, thermal expansions of fuel pellet and cladding and resultant gap shrinkages are appropriately taken into account for calculating temperature increments both across the gap (gap conductance) and over the fuel pellet by an iterative method.

A.2. Dimensional inputs

An etched transverse ceramograph of a medium burnup fuel pin is shown in Fig. 11, where eight distinct regions such as cladding tube, fuel-to-cladding gap (residual gap), peripheral region, dark ring, densified region, gas bubble region, columnar grain region, and central void are clearly observed. For the analysis the fuel restructuring are simplified into three regions (peripheral region including dark ring, equiaxed region: densified region and gas bubble region, and columnar grain region) as illustrated in Fig. 12. Cladding outer radii (r_{co}), cladding inner radii (r_{ci}), peripheral region radii (r_{fo}), equiaxed grain radii (r_{eq}), columnar grain region radii (r_{cg}), central void radii (r_{fi}) are measured in the ceramographs to make dimensional input data.

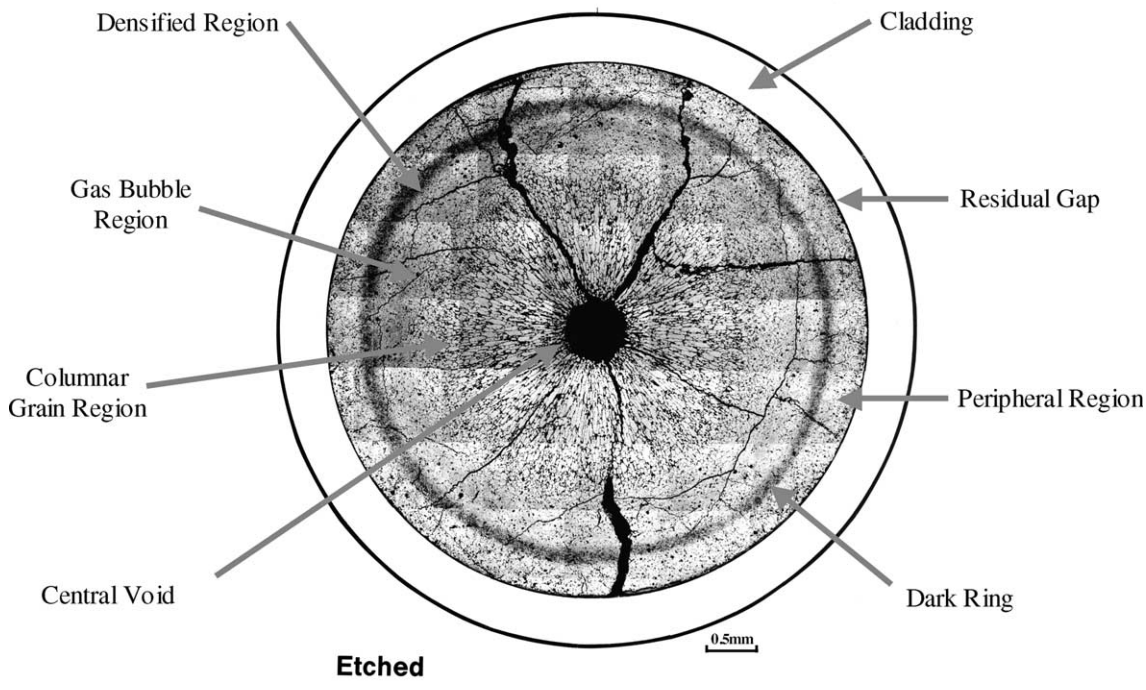

Fig. 11. A typical transverse ceramograph without the JOG evolution in a high burnup fast reactor type uranium–plutonium oxide fuel pin.

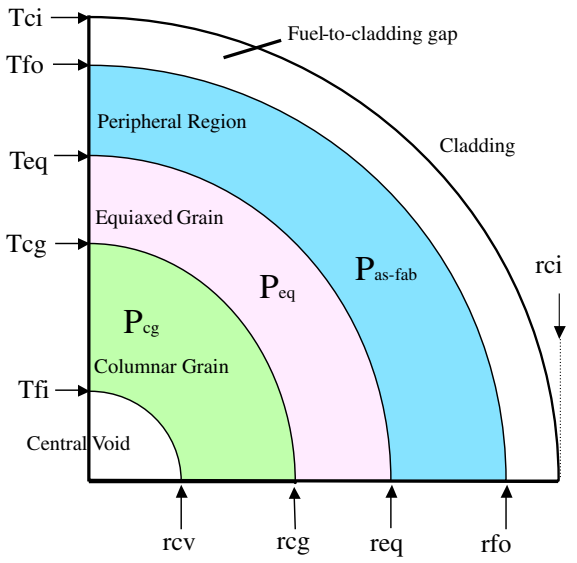

Fig. 12. Fuel restructuring modeled for the thermal analysis.

A.3. Heat conduction in fuel pellets

A corrective method for irradiation effects on thermal conductivity in uranium dioxide fuels proposed by Lucuta et al. [14] will be applicable for the FR-MOX fuels because of the similarity of both fuels [15]. Corrective factors by dissolved solid FP: F_1; precipitated solid FP: F_2 and radiation damage: F_3; porosity: F_4 are multiplied to the fully dense state of the fuel formulated as Eq. (A.1):

$$k = F_1F_2F_3F_4k_0, \tag{A.1}$$

where k is effective fuel thermal conductivity in W/mK, k_0 is fully dense state fuel thermal conductivity in W/mK. The PNC98 equation [16,17] for FR-MOX fuels is selected for k_0 as formulated in Eq. (A.2):

$$k_0 = \frac{1}{0.06059 + 0.2754\sqrt{2 - O/M} + 2.011 \times 10^{-4}T} + \frac{4.715 \times 10^9}{T^2}\exp\left(-\frac{16361}{T}\right), \tag{A.2}$$

where T is temperature in K, O/M is oxygen-to-metal (O/M) ratio. $F1$, $F2$ and $F3$ are the pragmatic correlations formulated by Lucuta et al. [14] as formulated in Eqs. (A.3)–(A.5):

$$F_1 = \left(\frac{1.09}{\beta^{3.265}} + \frac{0.0643}{\sqrt{\beta}}\sqrt{T}\right)\arctan\left(\frac{1}{\frac{1.09}{\beta^{3.265}} + \frac{0.0643}{\sqrt{\beta}}\sqrt{T}}\right), \tag{A.3}$$

$$F_2 = 1 + \frac{0.019\beta}{(3 - 0.019\beta)}\frac{1}{1 + \exp\left(-\frac{T-1200}{100}\right)}, \tag{A.4}$$

$$F_3 = 1 - \frac{0.2}{1 + \exp\left(\frac{T-900}{80}\right)}, \tag{A.5}$$

where β is burnup in atomic percent of heavy metal. Although an application range of the method is limited up to 1900 K [14], we assume to be capable of extrapolating at higher temperatures. For F_4, the modified Loeb correlation is selected as written in Eq. (A.6):

$$F_4 = 1 - \alpha P, \tag{A.6}$$

where P is volume fraction of porosity, α is a coefficient. Applicable coefficients for as-fabricated conditions are 2.5 for JOYO Mk-II driver fuel pellets and ranging from 1.6 to 2.1 for MONJU type fuel pellets as characterized by Inoue et al. [18,19]. Porosity volume of peripheral region assumes to be the same as as-fabricated one and that of columnar grain region be calculated by the Doi–Katsuragawa correlation written as Eq. (A.7):

$$P_{cg} = P_{as\text{-}fab}\left(\frac{1}{2.2\sqrt{\beta} + 2.0\beta^2 + 1.667} - 0.0082\beta + 0.4\right), \tag{A.7}$$

where P_{cg} is porosity volume fraction in columnar grain region, $P_{as\text{-}fab}$ is as-fabricated porosity volume fraction. Porosity volume fraction of equiaxed region: P_{eq} assumes to be the average of P_{cg} and $P_{as\text{-}fab}$. The effects of radial plutonium and oxygen redistribution phenomenon on the thermal conductivity are neglected in the analysis.

A.4. Fuel stoichiometry change

Contrary to water reactor fuels, stoichiometry changes should be considered, since FR-MOX fuels are intentionally fabricated in hypostoichiometry. Oxygen balances are calculated in consideration with fission yields and then calibrated by the experimental measurements of O/M ratios by X-ray diffraction. Only 'zirconium and niobium (Zr + Nb)', 'yttrium and rare earths (Y + RE)', and 'barium and strontium (Ba + Sr)' are assumed to contribute the oxygen balance in the fuel pellets, where 'Ba + Sr' are precipitated out with 'Zr + Nb' as gray phase: (Ba,Sr) $(Zr,Nb)O_3$ and remaining 'Zr + Nb' and 'Y + RE' are dissolved in the matrix. We can roughly estimate the effective thickness of the corrosion layers and oxygen consumptions by the actual measurements.

A.5. Heat transfer across fuel-to-cladding gaps

A heat transfer model across the gap established by Ross and Stoute [20] is applied for the analysis as is very

often the case with fuel pin performance analysis codes. In the model, heat flows across the gap through the following four parallel components; conduction, convection, radiation, and solid-to-solid contact, and then gap conductance is written as the sum of the components in Eq. (A.8):

$$H_{\text{gap}} = H_{\text{gas}} + H_{\text{rad}} + H_{\text{solid}}, \tag{A.8}$$

where H_{gas} is a component of the conduction and convection by filled gas, H_{rad} is that of the radiation, H_{solid} is that of the contact. The contributions of the radiation and convection are approximately negligible. As fuel-to-cladding contact would be unlikely after the JOG evolution under steady state irradiation conditions, the fuel-to-cladding contact contribution is not probable. The gap gas contribution is formulated in Eq. (A.9):

$$H_{\text{gas}} = \frac{k_{\text{mixed-gas}}}{R + \text{TJD} + \text{GAP}}, \tag{A.9}$$

where H_{gas} is gap conductance by gap gas contribution, $k_{\text{mixed-gas}}$ is thermal conductivity of mixed gas, R is effective roughness of cladding and fuel pellet surfaces (4.8 μm [21]), TJD is temperature jump distance at cladding and fuel pellet surfaces, and GAP is the radial gap width at power. The mathematical treatments by Bird et al. [22] and by Kennard [23] are available to calculate the $k_{\text{mixed-gas}}$ and TJD, respectively. Each region, except for the gap, is subdivided into ring meshes which thermally expand by the thermal expansion coefficient, and the accumulated radial increments are used to determine GAP. If the gap filler assumes to be cesium molybdate, $k_{\text{mixed-gas}}$ in Eq. (A.9) will be replaced by the following equation reported by Ishii and Mizuno [24,25] as written in Eq. (A.10):

$$k_{\text{Cs}_2\text{MoO}_4} = 0.0335 + \frac{148.11}{T} + 3.575 \times 10^{-10} T^3, \tag{A.10}$$

where $k_{\text{Cs}_2\text{MoO}_4}$ is thermal conductivity of fully dense cesium molybdate in W/mK. It should be noted here that cesium molybdate is a sort of solid or liquid medium for heat transfer and that the heat transfer is practically the sum of the conduction through both mixed gas and condensed materials. Condensed materials in the gap are always compressed by the fuel pellet, the assumption of fully dense state is reasonable.

References

[1] M. Tourasse, M. Boidron, B. Pasquet, J. Nucl. Mater. 188 (1992) 49.

[2] M. Tourasse, M. Boidron, B. Pasquet, in: Proceedings of International Symposium on Material Chemistry in Nuclear Environment, Tsukuba, Ibaraki, Japan, 12–13 March, 1992, p. 13.

[3] K. Maeda, T. Mitsugi, T. Asaga, in: Proceedings of International Workshop of Interfacial Effects in Quantum Engineering Systems: IEQES-96, Mito, Ibaraki, Japan, 21–23 August 1996, PB-04.

[4] M. Naganuma, K. Maeda, N. Nakae, J. Rouault, J. Noirot, G. Crittenden, C. Brown, in: Proceedings of 6th International Conference on Nuclear Engineering (ICONE-6), San Diego, California, USA, 10–15 May 1998, ICONE-6257.

[5] M. Naganuma, S. Koyama, T. Asaga, J. Noirot, D. Lespiaux, J. Rouault, G. Crittenden, C. Brown, IAEA-SM-385/24, 1999, in: Proceedings of International Symposium on MOX Fuel Cycle Technologies for Medium and Long-Term Deployment, Vienna, Austria, 17–21 May 1999.

[6] M. Katsuragawa, H. Kashihara, M. Akebi, J. Nucl. Mater. 204 (1993) 14.

[7] M. Inoue, T. Asaga, Japan Nuclear Cycle Development Institute Report JNC TN9400 2001-081, 2001 (in Japanese).

[8] K. Kamimura, S. Nagai, N. Tobita, M. Toyoshima, M. Suzuki, Y. Nogami, M. Ohtsu, M. Kajitani, S. Ishikawa, Y. Goto, Power Reactor and Nuclear Fuel Development Corporation Report PNC TN8410 92-080, 1992 (in Japanese).

[9] K. Katsuyama, K. Tatebe, I. Unno, S. Ukai, S. Iwanaga, 1994 Fall Meeting of the Atomic Energy Society of Japan, J37, Hokkaido, Japan, 28–30 September 1994 (in Japanese).

[10] K. Une, M. Hirai, K. Nogita, T. Hosokawa, Y. Suzawa, S. Shimizu, Y. Etoh, J. Nucl. Mater. 278 (2000) 54.

[11] C.T. Walker, T. Kameyama, S. Kitajima, M. Kinoshita, J. Nucl. Mater. 188 (1992) 73.

[12] K. Lassmann, C.T. Walker, J. van de Laar, F. Lindstrom, J. Nucl. Mater. 226 (1995) 1.

[13] C.E. Johnson, I. Johnson, P.E. Blackburn, C.E. Crouthamel, React. Technol. 15 (1972–1973) 303.

[14] P.G. Lucuta, H.j. Matzke, I.J. Hastings, J. Nucl. Mater. 232 (1996) 166.

[15] J.J. Carbajo, G.L. Yoder, S.G. Popov, V.K. Ivanov, J. Nucl. Mater. 299 (2001) 181.

[16] M. Inoue, T. Asaga, Japan Nuclear Cycle Development Institute Report JNC TN9400 98-005, 1998 (in Japanese).

[17] M. Inoue, J. Nucl. Mater. 282 (2000) 186.

[18] M. Inoue, T. Asaga, Japan Nuclear Cycle Development Institute Report JNC TN9400 99-005, 1998 (in Japanese).

[19] M. Inoue, K. Abe, I. Sato, J. Nucl. Mater. 281 (2000) 117.

[20] A.M. Ross, R.L. Stoute, Atomic Energy of Canada Limited Report AECL-1552, 1962.

[21] M. Inoue, T. Asaga, Japan Nuclear Cycle Development Institute Report JNC TN9400 2001-080, 2001 (in Japanese).

[22] R.B. Bird, W.E. Stewart, E.N. Lightfoot, Transport Phenomenon, Wiley, New York, NY, USA, 1960, p. 253.

[23] E.H. Kennard, Kinetic Theory of Gases, McGraw-Hill, New York, NY, USA, 1938, p. 311.

[24] T. Ishii, T. Mizuno, J. Nucl. Mater. 231 (1996) 242.

[25] T. Ishii, T. Mizuno, J. Nucl. Mater. 247 (1997) 82.